Fermi National Accelerator Laboratory

FERMILAB-Conf-86/52-E
[E-660]

The Application of Channeling in Bent Crystals to Charged Particle Beams *

Richard A. Carrigan, Jr.
Fermi National Accelerator Laboratory
P.O. Box 500, Batavia, Illinois 60510 U.S.A.

March 1986

* Presented at the NATO Advanced Research Workshop, Maratea, Italy, March 31 - April 4, 1986.

Operated by Universities Research Association, Inc., under contract with the United States Department of Energy

FERMILAB-CONS86/52-E660

THE APPLICATION OF CHANNELING IN BENT CRYSTALS TO CHARGED PARTICLE BEAMS

Richard A. Carrigan, Jr.*

Fermi National Accelerator Laboratory

March 1986

*Much of the work reported here has been done in cooperation with groups from Albany, Chalk River, Dubna, and New Mexico. The author would particularly like to acknowledge many discussions with S. Baker (Fermilab), J. Ellison (New Mexico), J. Forster (Chalk River), W. Gibson (Albany), I. Kim (Albany), S. Salman (An Najah), C. Sun (Albany), E. Tsyganov (Dubna), and R. Wijayawardana (Peradeniya).

BEAM DEFLECTION WITH BENT CRYSTALS

The first serious suggestion that channeling in bent crystals could be used to deflect charged particles was made by E. Tsyganov in 1976[1]. At that time he identified the possibility of using crystals for bending and focusing high energy beams. In 1979 a joint USSR-US team working at Dubna[2] observed the deflection of channeled particles for the first time. The observations were made at an energy of 8.4 GeV and reached angles of up to 26 milliradians. These results have since been confirmed by measurements at CERN[3] and at Fermilab[4-6]. Much of the emphasis of the CERN work, done at a momentum of 12 GeV/c, has been on axial bending and on Monte Carlo studies of the process. A particular feature of the Fermilab program is a wide range of momenta (12 GeV/c to 800 GeV/c) so that something can be said about the functional momentum dependence of dechanneling and so that longer crystals can be used without a major impact from dechanneling. Some work has also been done at Gatchina[7] near Leningrad at a relatively "low" energy of 1.0 GeV. This work particularly emphasizes feeding-in and feeding-out effects. All of these bending studies have been summarized in a recent review by Carrigan and Gibson.[8]

The basic bending process is almost obvious for a curved planar geometry. A positive particle inside the critical angle of the plane will follow the curved planes provided the curvature of the crystal is not too large. Dechanneling still occurs, due both to ordinary dechanneling, as well as certain features of the

bending process. The actual potential well in the channel is modified by a linear centrifugal barrier that depends on the local crystal curvature. Figure 1, from Kudo[9], shows how this occurs. At a small enough bending radius, the Tsyganov radius,

$$R_T = E/eE_c \qquad (1)$$

the centrifugal barrier exactly equals the depth of the normal (unbent) potential and particles no longer are deflected. Here E is the total energy of the particle and E_c is the interatomic field intensity at a distance from the plane of the crystal lattice where the trajectory of the particle no longer remains stable due to its interactions with individual atoms. In practice, the process is no longer practically useful well before the Tsyganov radius is reached.

Axial bending is more complicated. A simple picture is to think in terms of the axis as a sum of planes. The orientation of some of these planes is such that only a component of the centrifugal force acts to deflect the particles so that multiple beams are deflected away from the primary beam. Figure 2, based on Bak, et al.[3], illustrates the multiple beams diverging from an axially aligned crystal.

Even more complicated is the question of negative particle bending. There the negative particle must be attracted by a single string so the effective critical angle is limited. At the same time it moves in a region where dechanneling is high. There appears to be no evidence of negative particle deflection to the full extent of the crystal bending angle in an experiment.

From the standpoint of practical applications the actual behavior of the potential and its inter-relationship to both ordinary and bending dechanneling is complex. Since the potential narrows as the crystal is bent, the critical angle also becomes smaller. In addition the center of gravity for the channeling orbits moves into regions of higher charge density. As a result, the dechanneling length should decrease. Finally the characterization of the mechanical details of crystal bending is often not at all straightforward.

The beam transmission through a bent crystal depends on several factors:

1) Angular acceptance: For a planar geometry the angular acceptance in the direction of the bend corresponds to the critical angle, ψ_{pb}. While trajectories are accepted out to roughly $\pm\psi_{pb}$, the critical angle corresponds approximately to the 50% transmission points or the full width at half maximum. Note that a subscript b has been added to indicate that this is the critical angle at the point of greatest bending. Perpendicular to the bend all angles will be transmitted for practical geometries.

   The angular acceptance in the direction of bend will be proportional to $\sqrt{Z}$ since it is proportional to the critical angle.

2) Spatial acceptance: To a first approximation the spatial acceptance in the direction of the bend is t, the crystal thickness. Since the crystal is being bent in that

direction, it is ordinarily quite thin, perhaps 0.5-1.0 mm. Two factors can make the acceptance less. If the planes are not properly aligned with the body of the crystal, some trajectories will leak out of the sides and a misalignment correction should be applied. For example, a 50 mm long crystal misaligned by 5 milliradian will have an equivalent thickness loss of 0.25 mm. The effective thickness can also be reduced due to local curvature resulting from the jig used to bend the crystal. This will be discussed in more detail later.

Perpendicular to the bend the spatial acceptance can nearly always be made large enough to accommodate the whole beam.

Factors 1) and 2) can be combined to give a fractional angular and spatial acceptance for the incident beam. The effective phase space acceptance of the crystal in the direction of bend is

$$\phi_b^{50} = 2\sqrt{\frac{\ell n\ 2}{\pi}}\ \psi_{pb}\ t \qquad (2)$$

Here ϕ_b^{50} is the phase space to compare to a 50% beam phase space contour. The crystal thickness is multiplied here by $2\sqrt{(\ell n 2)/\pi}$. This assumes the beam spatial distribution is Gaussian and substantially wider than the crystal thickness.

Figure 3 illustrates the typical phase space of a particle beam at several places along the beam as well as the crystal phase space acceptance[10]. Note that while the beam phase space is elliptical the crystal acceptance is rectangular because even at the edge of the crystal, all angles within the channel are accepted. Characteristically the crystal phase space is one percent of the beam phase space.

3) Normal dechanneling: As a particle moves through a bent crystal "ordinary" dechanneling takes place. For planar dechanneling in silicon crystals, most of this comes from interactions with electrons. As noted earlier, the distribution of electrons sampled in a bent crystal is different and denser than an unbent crystal because the trajectories are shifted closer to the nuclear planes. Tarantin, et al.[11-12], have studied this behavior using several different electron densities in the Fokker-Planck equation. Figure 4 shows how the dechanneling length drops for small radii of curvature. Figure 5 illustrates how this effect varies with energy for different radii of curvature.

There is also a further complicating factor. At MeV energies dechanneling lengths are ordinarily calculated and measured with beams with angular diverges much smaller than the critical angles. This is no longer true at multi-hundred GeV energies since the beam angular width is normally much larger than the critical angle.

Thus scaling up low energy dechanneling lengths purely on a kinematic basis will overestimate the high energy dechanneling length. Figure 6 shows how this effect depends on the beam angular divergence normalized to the critical angle. By the time the beam angular divergence is equal to the critical angle, the dechanneling half length has been reduced by a factor of 2. Figure 7 summarizes some of the experimental and theoretical estimates of ordinary dechanneling lengths and illustrates this effect. If all these experimental points are properly averaged to give a dechanneling length for a beam with an angular distribution equal or larger than the critical angle, the length (1/e) at 100 GeV/c for Si is 70 mm ± 15 mm.

Finally--note that the dechanneling fractions should be estimated using the diffusion equation. Here however we use an exponential to estimate the dechanneled fraction. Both the low energy[14] and the high energy data[16] suggest this is a good approximation. For example, Fig. 8 from Sun, et al.[16], shows the dechanneling as a function of crystal length after the point of maximum bend at 8.4 GeV. This nicely follows an exponential curve.

With these caveats the fractional dechanneling due to "ordinary" dechanneling is:

$$f_d = e^{-\frac{s}{\lambda_0}\left(\frac{p_o}{p}\right)} \qquad (3)$$

where λ_0 is the phenomenological dechanneling length determined at a momentum p_o and s is the length of the crystal.

4) Bending dechanneling: Theoretical treatments of bending dechanneling have been developed by Ellison[18], Kudo[9], and Kaplin and Vorobiev[19]. The only effort to measure these directly appears to have been by the Albany-Chalk River-Fermilab-New Mexico group[4] operating at energies on the order of a hundred GeV. This group noticed significant losses due to the middle pin of a 3-point bending jig as illustrated in Fig. 9. These losses were attributed to local distortion in the crystal near the center pin. Indeed they were shown to be due to trajectories on the center pin side of the crystal. By using this effect as a dechanneling spectrometer, it was possible to measure losses directly. Unfortunately there is substantial uncertainty in properly estimating the local curvature in the crystal.

Figure 10 shows the experimental points and compares them to the (111) plane in silicon. It is unfortunate that the (111) orientation involves both wide and narrow planes. This has led to complications both in the experiments and the theory. In practice different

choices for charge distribution lead to fairly large changes in the theoretical predictions. About the best that can be said is that the general character of the experimental measurements agree with the theory.

For the transmission curves that follow the dechanneling fraction has been approximated by a linear function:

$$f_d^a = \frac{1}{3}\,\frac{p}{R} \qquad (4)$$

where p is the momentum in GeV/c and R is the smallest radius of curvature in cm. As an approximation this can be used for either the (110) or (111) planes in silicon since theoretical uncertainties are more than the expected differences between the planes. For the transmission curves given here R is taken as the smallest global radius of curvature over the length of the crystal. Pin effects are treated later for clarity.

5) Surface acceptance: Not all the particles within the critical angle will be accepted. Figure 11 shows a schematic of the phase space that might be accepted. For a uniform angular illumination this gives rise to an acceptance of $E_c = 0.64$ for silicon as calculated by Wijayawardana[6] if a is equal to the Thomas-Fermi screening distance. Wijayawardana found the raw experimental value is about 0.3 but argues that the

corrected experimental value is 0.55. In any case this is smaller than planar minimum yields at low energy suggest. In that regime beam angular distributions are typically much less than the critical angle. Note that this surface acceptance is a function of the mechanism that gives rise to the closest distance of approach, a. High energy data suggests this is a fairly large number so that the surface acceptance may be smaller than expected.

For these simple assumptions the transmission is

$$E = E_c \left(1 - \frac{p}{3R_m}\right) e^{-\frac{s}{\lambda_o}\,\frac{\rho_o}{p}\,\frac{\phi_b^{50}}{\phi}} \qquad (5)$$

where ϕ is the 50% profile emittance of the beam. (Remember that a full treatment would replace the approximation within the parentheses with a correct functional form from a theory such as Kudo or Ellison.)

Figure 12 shows how this transmission behaves as a function of length for a range of momenta, a fixed angle of bend (10 mrad), and λ_o = 55 mm at 100 GeV/c. If the crystal is too short, the radius of curvature is smaller than the Tsyganov radius and no particles are transmitted. As the length increases, the transmission initially rises and then drops as the particles begin to dechannel. High energies require longer crystals.

Figure 13 illustrates how the transmission changes with angle for a crystal with a fixed length of 5 cm and a range of momenta. A long crystal is chosen to emphasize the behavior at high energy. Obviously the transmission is highest for zero bend. Transmission drops with increasing angle and goes to zero when the Tsyganov radius is reached. As the energy increases, the transmission initially rises. This is because the effect on the increasing dechanneling length is larger than the decreasing critical angle. In the 200-400 GeV region dechanneling becomes negligible and the decreasing solid angle starts to lower the acceptance as the energy increases.

How large a bending angle could be obtained using a crystal? At high momenta the dechanneling length is $\lambda = (\lambda_o/p_o)p$. Using the approximation (4) and assuming $f_d^a = 1.0$, $R_T^a = (pv)/3$ for silicon. The maximum angle of bend is then

$$\theta_{max} = \frac{\lambda}{R} \tag{6}$$

For silicon this is about 150 milliradians. (The largest bend reported so far is 52 milliradians by Bak, et al.[3].) For tungsten R_T^a is 1/8 of the silicon value[18] while the dechanneling length might be 50% higher. Thus $\theta_{max} = 2$ radians for tungsten.

Up to this point the local distortions around the pins in the bending jig have been ignored. However, these can be very significant. Figure 14 taken from Frocht[20] shows the stress pattern in a beam under a concentrated load using the photoelastic technique. The stress concentration is obvious. Salman[5] and Wijayawardana[6] have used the Wilson-Stokes approximation to derive the radius of curvature near such a concentrated load. Wijayawardana gets:

$$\rho(y) = -\frac{8P}{0.141\pi E_y t^2}\left[\frac{y^2}{2t^2} - \ln\left(1.648\,\frac{y}{t}\right)\right] \tag{7}$$

where ρ is the local radius of curvature, E_y is Young's modulus, t is the thickness of the slab, and y is the distance across the beam from the pin. The stress per unit width, P, on the crystal is:

$$P = \frac{E_y}{3(1-\nu^2)}\, t^3\, \frac{\theta}{(L^2 - b^2)} \tag{8}$$

where θ is the total bend of a crystal in a four-point jig of length L with the two center pins separated by a distance b, and ν is the Poisson ratio. The case for a three-point jig can be obtained by setting b=0 and doubling P.

Figure 15 illustrates how this local curvature varies across a crystal. The global curvature is also indicated. The total radius of curvature (also shown) is the sum of both the local and global curvature. The bending efficiency across the crystal (using the earlier approximation) is also indicated in the figure.

The net effect of this local curvature can be obtained by integrating across the crystal, effectively integrating across Fig. 15. In order to get a factor that can be used as a

multiplier for formula 5 and Figs. 12 and 13, this efficiency has been divided by the bending efficiency for the global radius of curvature. Figure 16 illustrates the behavior of this pin correction as a function of crystal thickness and momentum. The effect is surprisingly insensitive to crystal thickness. Note however that the stress is increasing as the cube of the crystal thickness so that it is not practical to increase the thickness indefinitely.

So far these discussions have been addressed to the middle pins. The stresses on the middle pins for a four-point jig are less than in a three-point jig suggesting the middle pin losses should be less. Indeed this has been true in the Fermilab experiments. However, there must also be losses on the first pin. These are much more difficult to observe. These losses should be higher for a four-point jig. When the losses are combined, a three-point jig might turn out to be more satisfactory in some situations.

Following an idea due to I. Mitchell, the Chalk River-Fermilab-New Mexico group has demonstrated bending in crystals permanently bent by sputtering zinc oxide on the convex side. Such crystals would need no bending jig. This might be particularly desirable for extraction elements. On the other hand, it would not be possible to adjust the deflection angle.

SOME BENDING APPLICATIONS THAT HAVE BEEN TRIED

MB Beam at Fermilab: The first application of a crystal as a secondary beam element has been at Fermilab in the Meson-Bottom beam[6,21]. This is the test beam that has been used for much of the recent channeling work at FNAL. The front end of the beam contains two 3.05 m long dipole septum magnets giving a net downward deflection of 8.9 mrad. In beam parlance a septum magnet is a magnet with a thin side (often a current sheet) that is slipped in between two narrowly separated beams to kick them apart. The MB magnetic septa limited the beam momentum to below 225 GeV/c. As can be seen from Fig. 12, such a crystal can deflect some beam up to 400 GeV. When this crystal septum was tried, 400 GeV was the primary energy of the accelerator so operation of the beam at that energy could potentially produce a much more intense beam.

Figure 17 shows the septum silicon crystal mounted in place in a four-point bending jig. A (110) plane lies in the horizontal plane of the crystal. Planar channeling was used rather than axial. While the critical angle is larger for axial channeling and the dechanneling length is longer, axial channeling feeds particles in to several different beams due to the presence of skew planes as noted earlier. Indeed, Bak, et al.[3] seem to find negligible bending inside the axial critical angle. In addition the beam angular divergence is large enough that much of the useful deflected beam would come from planar channeling in either case. Finally axial channeling requires a

second round of alignment in a situation where alignment can be difficult.

In practice the crystal bending angle was set and the plane was aligned using the energy loss technique in the normal channeling drift chamber location. The crystal was then carefully relocated into the septum position and the MB beamline was set up using the magnetic septa. Next the magnetic septa were turned off and the crystal rotated to look for a peak in beam transmission. Figure 18 shows the crystal alignment curve at 400 GeV/c. Note the absence of background. The final crystal position differed from the surveyed position by half a milliradian. Finding the plane for the first time in the Front End Hall took between 10 and 20 accelerator spills.

In this case locating the crystal plane turned out to be straightforward. Note that the implanted detector was not used to align the crystal. Instead alignment was achieved by making use of the fact that the only way beam could be transmitted down the beam was when the crystal was aligned. At Fermilab this method is called the Kim technique after I-J. Kim, who first suggested it. There are obvious problems--the downstream beam detectors must be free of background, and the crystal bend angle must be set accurately enough so that particles will be captured by the beam.

Several alternative techniques were tested when the septum was tried for the first time. Figure 19 shows a detector energy spectrum near the septum position. While there is a hint of a

Landau peak, the accidental background from other beamlines overwhelms it so that the technique of using low energy loss is impossible to use. A very tiny scintillation counter was also attached to the septum stand. It was accurately positioned so it was out of the central beam and would only count in coincidence with a small upstream counter when the crystal was aligned. This also had a problem with very high accidental counting rates.

The crystal was able to transmit beam up to 400 GeV/c. This was nearly twice the momentum that the beam ordinarily transported. Beam safety considerations (basically fear that the crystal would work too well) limited operation in this mode. With the safety constraints, the crystal deflected 10,000 protons/spill.

The beam transmission in the test location was 0.03% at 200 GeV/c. The expected transmission based on Eq. (5) was 0.15%. At this point it is not entirely clear what the differences are due to, but some of the factors could include pin effects, misalignment of crystal planes in the crystal body, and over-estimation of the surface acceptance.

During the initial run no particular effort was made to optimize the beam for crystal operation. However, certain features of the crystal can potentially be exploited. In particular, in the bend direction the beam angular divergence and size are both very small. Figure 20 shows the beam optics with the quadrupoles off. The vertical beam divergence is small and there is a lack of momentum recombination. Figure 21 illustrates

a 400 GeV tune with horizontal point-to-point optics and momentum recombination. Clearly substantial flux gains can be achieved in this way.

NE Beam at Fermilab: One of the interesting possibilities that has developed for application of bent crystals is as a beam attenuator. At Fermilab much effort is now concentrated on exploitation of the 800 GeV Tevatron beam. External area beams of this sort are very intense since they come directly from the accelerator. On the other hand much of this work is focused on short-lived particles and often requires special slow detectors such as emulsions and bubble chambers. Thus a clean technique is needed to cut the intensity of the beam. Collimators and multiple scattering attenuators tend to be difficult, introduce background, and may be unable to provide enough of a reduction.

Two experiments have recently been running in the Neutrino East (NE) proton beam at Fermilab. The upstream experiment, E711, is a high intensity (10^8-10^9 particles/spill) counter experiment, while the downstream experiment, E653, is a low intensity (10^4-10^5 particles/spill) emulsion spectrometer. Both of these require the full 800 GeV Tevatron energy. Figure 22 shows a schematic of the layout of the experimental area. It was possible to provide sufficient attenuation to run the experiments simultaneously by placing a bent crystal between the two experiments to replace forty feet of magnets bending the beam through 3.14 milliradians.[10]

The same practice of prealignment in a test beam area was followed that was used in MB. Because of uncertainties about the operating value of the E711 magnetic spectrometer, it was necessary to compensate the crystal bend by using the original bending magnets as a trim. The crystal bend angle was 3.67 ± 0.17 milliradians. The crystal orientation was determined by measuring the beam count rate in the E653 apparatus and by observation with a segmented wire ionization chamber (SWIC) located at E653. The plane was found to be 0.26 milliradians away from the predicted location as established by test beam running, surveying, and laser positioning. This is consistent with the expected errors. Alignment took approximately 40 minutes, corresponding to 130 25-microradian steps. Figure 23 shows the alignment curve while Fig. 24 shows the beam in the SWIC. The beam spot at E653 is quite small as it should be in light of the critical angle at 800 GeV/c. The background is much higher than in MB because there is no downstream sweeping magnet to clear out the original undeflected beam. Note that the undeflected beamline is only 0.4 m from the crystal deflected line at the E653 target. The beam dump just downstream of the crystal was also relatively unsophisticated.

The observed beam transmission was 0.54×10^{-3}. The expected transmission on the basis of formula (5) is 3.2×10^{-3}. As with MB, there are a number of possibilities that could explain the reduction. It may be noteworthy that the reductions are about the same in the two cases.

This application is at the highest energy that channeling effects have been observed. While the work was being carried out it was sobering to realize that this was a factor of a million times the energy that had been used for many of the original channeling experiments with a concomitant critical angle a thousand times smaller.

An interesting possibility for an application was noticed in the course of the NE work. This was the possibility for the use of a bent crystal as a beam phase space monitor. Since the critical angle for channeling is much smaller than the beam angular divergence, the crystal provides a delicate angular probe. Figure 3 illustrates the process. The vertical lines show scans at different positions across the beam spot. There is some evidence that the beam angular divergence changed accordingly. In practice it would be difficult to measure angular divergence directly in another way in an intense beam.

MT Beam at Fermilab: Not every application of crystal channeling has worked at Fermilab. An attempt was made to use a crystal in the front end of the MT beam to replace a pinhole collimator and a 0.88 mrad west bend. The plan was to provide a reduction of 10^6 in beam intensity so the Little European Bubble Chamber (LEBC) could operate in the beam. The attempt failed for several reasons. The available monitors were not free enough of background to detect the small signal. In addition the beam system was not sufficiently forgiving so that an error in setting the bend of 0.1 mrad could be tolerated. The combination of

these two problems and the need to find the plane in a period when the accelerator was just coming on and operating poorly proved to be overwhelming. The crystal was abandoned for a beryllium attenuator.

Extraction from the JINR Synchrophasotron: Use of a bent crystal as a beam extraction device was proposed by G. D. Koshkarev[22] in 1977. The first and only extraction of beam from an accelerator using a bent crystal was done at Dubna[23] around 1983. The extraction arrangement is illustrated in Fig. 25. A crystal (10 mm long and 0.4 mm thick) on the inside of the first accelerator straight section deflected the beam 35 milliradians toward an extraction channel on the outside of the second straight section. The crystal was mounted and bent by gluing it to a cylindrical aluminum surface. Aiming of the extracted beam was achieved by varying the equilibrium radius of the internal beam.

Figure 26 shows the crystal orientation as a function of internal energy. The width of the peak in the orientation curve is related to the beam distribution in the accelerator. The background is due to secondary radiation in the counters.

The effective beam transmission was 10^{-4} and was determined mainly by the geometrical size of the detector. One improvement that has been considered at Dubna is the use of layers of crystals to increase the transverse area. It is probably also true that both the required bend and the length of the crystal served to diminish the transmission.

SOME FUTURE POSSIBILITIES

Booster to Antiproton Source Line at Fermilab: During main accelerator downtimes it is useful to feed 8 GeV beam from the Fermilab Booster into the new antiproton storage ring complex. The Booster beam intensity is naturally high, 10^{12} protons/spill. For some applications, a much less intense beam is desirable. At present this is being accomplished with a multiple scattering attenuator. A bent crystal has been considered and may still be tried. Two factors must be taken into consideration--a short crystal is desirable and adequate provision must be made for alignment. It is estimated that an available crystal could give a transmission of 0.4×10^{-4}.

Other Secondary Beamlines at Fermilab: Several more applications similar to M-B and N-E have been considered but have been discarded. In part this has to do with uncertainties about a new technology and fear that alignment problems may be very difficult. In general no one is prepared to face the possibility of failure in a programmatic situation.

An obvious possibility would be a facility with many test beams produced by a series of crystals. This might be possible if the experimental area was a clean slate. Existing beam paths are such that this arrangement is not possible.

The Superconducting Super Collider: A 20 TeV hadron collider, the SSC, is under serious discussion in the U.S. As envisioned, this machine makes no provision for an external beam. Sun et al.[24] have considered how a crystal could be used. The

critical angle at 20 TeV is about one microradian. This may seem like a small angle but the beam divergence in a long straight section is expected to be 0.14 microradians so everything would be channeled. Sun et al. estimate the dechanneling length to be 12 m in silicon. On the other hand, the Tsyganov radius is 32 m. They suggest using a 48 microradian bend with a 10 cm long crystal to get better than 90% transmission. The 48 microradian bend is used to clear a Lambertson magnet placed halfway through the 1000 m straight section.

If 10% of the 10^{14} circulating beam is used over a ten hour period, one could obtain an external beam of 3×10^{8} particles/second. This is not a particularly intense beam. Sun et al. have also suggested techniques for getting more intense beams when the beam is cleared out of the machine every ten hours.

The alternative to a crystal is a very long electrostatic septum using thin wires. The required length would be hundreds of meters. There are several grave difficulties with the wire septum scheme including accelerator aperture considerations, wire radiation damage, and the practical problem of properly aligning the wires.

Recently De Rujula, et al.[25] have speculated on possible practical applications of multi-TeV accelerators. They suggest such accelerators could be used for geological exploration for minerals and petrochemicals and for measuring the density profile of the core of the earth. This would be done by extracting the

beam from the accelerator, targeting it to produce mesons, and letting the mesons decay in a long tunnel (typically 1 Km) to produce high energy neutrinos. For resource exploration the extracted beam must be bent and fanned through 5^{o}-10^{o}. For exploration of the center of the earth it must be bent 90^{o}. Four significant technology leaps are needed--a multi-TeV accelerator, an extraction technology, a bending snout, and a decay tunnel. Figure 27 shows a fanciful conception of how this could be realized for an ocean-going accelerator. Potentially bent crystals could be used for two of the four required technologies. As noted earlier, the maximum bending angle for good tungsten crystals is two radians. This would require an extremely good tungsten crystal 30-50 cm long. At present tungsten crystals are on the order of 1 cm long with large mosaic spreads.

With a good crystal it might literally be possible to deflect particles down toward the center of the earth. Several deep shafts on different chords of the earth, something like large diameter oil wells, would be needed for the meson decay tunnels.

Crystals as Focusing Elements: An interesting possibility is the use of bent crystals to form quadrupoles. Figure 28 illustrates how this might be done by making thin slices in a block[26]. Particles moving along the planes would be focused in one direction. Two sets of blocks could produce horizontal and vertical focusing. An alternative technique would be to clamp one end of a block to near the elastic limit. Sun and Lou[27] have

achieved compressions of 5 parts in 10^{4} with the jig shown in Fig. 29. (The elastic limit is 7 parts in 10^{4}.) For a given compression the shortest focal length is achieved with the shortest crystal. On the other hand the radius of curvature becomes shorter so there is more bending dechanneling.

Some feeling for the shortest possible focal length that might be achieved can be gained by considering that all the effect of a compression at the end of a crystal can be approximated by a circular arc. In that case the focal length is

$$f = \frac{1}{2}\sqrt{\frac{R\,t}{K}} \tag{9}$$

where R is some radius, say the Tsyganov radius, t is the thickness of the crystal, and K is the maximum fractional compression. The effective curved length of the crystal is

$$L = \sqrt{t\,K\,R} \tag{10}$$

For the sake of realism consider a radius that is five times the Tsyganov radius. At 100 GeV in silicon the Tsyganov radius is 160 mm. For a 1 mm thick crystal, with $K = 5 \times 10^{-4}$ the focal length is 63 cm. The curved portion of the crystal is 0.6 mm long, very short. This points up the fact that the approximation may be very optimistic. Indeed Sun and Lou estimate a typical focal length might be 500 cm. Now 63 cm may seem to be a very short focal length. For the most obvious possibility, short-lived particle beams, it is far too long since the

characteristic mean decay path for a D^+ meson at 100 GeV is 1.5 cm.

Another problem is the requirement of an incident beam that is parallel to within the critical angle. This difficulty might be ameliorated by using an active detector built into the crystal and selecting on low energy loss.

Short-Lived Particle Beams: As noted above, particles with charm and beauty travel only a very short distance before decaying. With a bent crystal, it should be possible to deflect these particles on the order of fifty milliradians before they decay, well out of the forward production cone. This could give a substantially enriched sample of short-lived particles if the long-lived particles in the same channel continue around the bend as illustrated in Fig. 30. On the other hand, dechanneling of long-lived particles may constitute a serious dilution. For planar geometries, angular acceptance is on the order of 1% of the production distribution. Note that at high energies, charm-particle production is expected to be reasonably copious. The problem lies more in separating particles, that is to say, enrichment is important.

Short-Lived Particle Magnetic Moment Measurement: Pondrom[28] has noted that the electric field of a crystal transforms into a magnetic field in the rest frame of a moving particle. The particle spin will precess around the magnetic vector. For a polarized process it is possible to measure the precession in the same way as has been done for strange particles. Effective

fields in bent crystals are sufficient to precess a magnetic moment several radians in 1 cm. Kim[29] has reviewed these possibilities in detail.

Sun has covered short-lived particle beams and magnetic moment measurements elsewhere in this volume.

THE FUTURE AND WHAT TO DO ABOUT IT

Channeling in bent crystals works! The process is limited by small angular acceptances and dechanneling considerations. However, these factors become somewhat more tractable as the energy is raised.

The basics of the process have been explored over a wide energy range and crystals have been used for several applications. This work has not been easy--proper crystals are difficult to fabricate and properly position in beams. More information and analysis is still needed in several areas. More data on crystals other than silicon is needed. Both germanium and tungsten (if proper crystals could be fabricated) should work better than silicon. More precise information with concrete estimates of the uncertainties is needed on dechanneling lengths, bending dechanneling, and "ordinary" dechanneling in bent crystals. In particular it would be useful to measure all these effects over a range of energies (10-200 GeV), angles (4-30 milliradians) and crystals lengths for both silicon and germanium with high statistics in one well functioning apparatus.

Another factor may need more investigation. This is the relationship between planar and axial bending. It has already been explored in some detail by Bak, et al.[3] at 12 GeV/c both experimentally and with Monte Carlo calculations. As noted earlier, their Fig. 12 suggests that there is no true axial bending, that is bending of particles within the axial critical angle. However, there is a substantial part in the donut region extending from one to five times the critical angle where enhanced capture may be present. The effect is essentially planar beyond five times the critical angle. The fractional transmission does not vary particularly over these regions, but "feed in" from a wider azimuthal range may favor this quasi-axial case. More information is still needed, particularly at multi-hundred GeV where bending dechanneling becomes stronger. This issue also needs to be understood in practical terms. Real beams, even in the hundred GeV regime, tend to have angular divergences on the order of 100 microradians.

Theoretical work is needed in the dechanneling area. This is particularly true in that the potential in a bent crystal is distorted so that increasing the bending is in some sense like raising the atomic number of the crystal. Ordinary and bending channeling need to be integrated. Careful attention needs to be paid to the functional relations between crystals of different materials.

In summary, channeling with bent crystals is a process with limitations but also tantalizing possibilities. More detailed fundamental information is needed to reach out toward more applications. Hopefully this information can be developed over the next several years.

REFERENCES

1. E.N. Tsyganov, Fermilab TM-682, TM-684, Batavia, 1976.

2. A.F. Elishev, N.A. Filatova, V.M. Golovatyuk, I.M. Ivanchenko, R.B. Kadyrov, N.N. Karpenko, V.V. Korenkov, T.S. Nigmanov, V.D. Riabtsov, M.D. Shafranov, B. Sitar, A.E. Senner, B.M. Starchenko, V.A. Sutulin, I.A. Tyapkin, E.N. Tsyganov, D.V. Uralsky, A.S. Vodopianov, A. Forycki, Z. Guzik, J. Wojkowska, R. Zelazny, I.A. Grishaev, G.D. Kovalenko, B.I. Shramenko, M.D. Bavizhev, N.K. Bulgakov, U.U. Avdeichikov, R.A. Carrigan, T.E. Toohig, W.M. Gibson, I.J. Kim, J. Phelps, C.R. Sun: Phys. Lett. 88B, 387 (1979).

3. J. Bak, G. Melchart, E. Uggerhój, J.S. Foster, P.R. Jensen, H. Madsbóll, S.P. Møller, H. Nielsen, G. Petersen, H. Schiótt, J.J. Grob, P. Siffert: Phys. Lett. 93B, 505 (1980); J.F. Bak, P.R. Jensen, H. Madsbóll, S.P. Møller, H.E. Schiótt, E. Uggerhój, J.J. Grob, P. Siffert, Nucl. Phys. B242, 1 (1984).

4. W.M. Gibson, I.J. Kim, M. Pisharody, S.M. Salman, C.R. Sun, G.H. Wang, R. Wijayawardana, J.S. Forster, I.V. Mitchell, T.S. Nigmanov, E.N. Tsyganov, S.I. Baker, R.A. Carrigan, T.E. Toohig, V.V. Avdeichikov, J.A. Ellison, P. Siffert, Nucl. Instrum. Methods B2, 54 (1984); presented at Int. Conf. Atomic Collisions in Solids, Bad Iburg, July 1983; S.I. Baker, R.A. Carrigan, C. Crawford, T.E. Toohig,

W.M. Gibson, H. Jin, I.J. Kim, M. Pisharody, S. Salman, C.R. Sun, G.H. Wang, R. Wijayawardana, J.S. Forster, H. Hatton, I.V. Mitchell, Z. Guzik, T.S. Nigmanov, E.N. Tsyganov, V.V. Avdeichikov, J.A. Ellison, P. Siffert, Phys. Lett. 137B, 129 (1984).

5. S.M. Salman, "Deflections of High Energy Channeled Charged Particles by Elastically Bent Silicon Single Crystals," Thesis, State University of New York at Albany (1982).

6 R. L. Wijayawardana, "Application of a Crystal Septum to Replace a Magnet in a Charged Particle Beam... ," Thesis - State University of New York at Albany (1985).

7. V.A. Andreev, V.V. Baublis, E.A. Damaskinskii, A.G. Krivshich, L.G. Kudin, V.V. Marchenkov, V.F. Morozov, V.V. Nelyubin, E.M. Orishchin, G.E. Petrov, G.A. Ryabov, V.M. Samsonov, L.E. Samsonov, E.M. Spiridenkov, V.V. Sulimov, O.I. Sumbaev, V.A. Shchegel'skii, Pis'ma Zh. Eksp. Teor. Fiz. 36, 340 (1982) [English Transl.: Sov. Phys.-JETP Lett. 36, 415 (1982).]

8. R.A. Carrigan, Jr. and W.M. Gibson, in "Coherent Radiation Sources," ed. A.W. Saenz and H. Uberall (Springer-Verlag-Heidelberg 1985).

9. H. Kudo, Nucl. Instrum. Methods 189, 609 (1981).

10. S.I. Baker, R.A. Carrigan, Jr., R.L. Dixon, H.C. Fenker, R.J. Stefanski, J.S. Forster, R.L. Wijayawardana, and S. Reucroft, Fermilab 86/20 (1986). To be published in Nucl. Instr. and Methods A.

11. A.M. Taratin, Yu.M. Filimonov, E.G. Vyatkin, S.A. Vorobiev, Phys. Status Solidi (b) 100, 273 (1980).

12. A.M. Taratin and S.A. Vorobiev, Phys. Stat. Sol. 107b, 521 (1981).

13. "Charged Beam Interaction with Solids," Y.H. Ohtsuki (Taylor and Francis--London--1983).

14. S.U. Campisano, G. Foti, F. Grasso, M. LoSavio, and E. Rimini, Rad. Effects 13, 157 (1972).

15. L.C. Feldman and B.R. Appleton, Phys. Rev. B8, 935 (1973).

16. C.R. Sun, W.M. Gibson, I.J. Kim, G.H. Wang, N.K. Bulgakov, N.A. Filatova, A. Foryeki, V.M. Golovatyuk, Z. Guzik, R.B. Kadyrov, T.S. Nigmanov, V.D. Riabtsov, A.B. Sadovsky, M.D. Shafranov, I.A. Tyapkin, E.N. Tsyganov, A.S. Vodoplanov, J. Wojtkowska, N.I. Zimin, R.A. Carrigan, Jr., T.E. Toohig, and M.D. Bavizhev, Nucl. Instr. and Meth. B2, 60 (1984).

17. J. Forster, private communiction.

18. J.A. Ellison, Nucl. Phys. B206, 205 (1982). See also J.A. Ellison, S.T. Picraux, Phys. Lett. 83A, 271 (1981).

19. V.V. Kaplin and S.A. Vorobiev, Phys. Lett. 67A, 135 (1978).

20. M.M. Frocht, Photo Elasticity, Vol. 2 (Wiley, New York, 1984).

21. S.I. Baker, R.A. Carrigan, Jr., R. Schailey, T.E. Toohig, W.M. Gibson, I.-J. Kim, F. Sun, C.R. Sun, V. Tanikella, R. Wijayawardana, J.S. Forster, H. Hatton, I.V. Mitchell,

and J.A. Ellison, Nucl. Instr. and Meth. A234, 602 (1985). See also R.A. Carrigan, Jr., Fermilab FN-362 (1982).

22. G.D. Koshkarev, ITEP, Preprint #30 (1977).

23. V.V. Avdeichikov, V.N. Buldakovskii, A.V. Bychkov, A.S. Vodop'yanov, I. Voitkovska, V.M. Golovatyuk, V.P. Grigor'yev, Z. Guzik, V.P. Zabolotyn, N.I. Zimin, I.B. Issinskii, R.B. Kadyrov, B.K. Kuryatnikov, L.G. Makarov, E.A. Matyushevskii, V.A. Monchinskii, T.S. Nigmanov, S.A. Novikov, V.G. Perfeev, V.D. Ryabtsov, A.B. Sadovskii, V.G. Timofeev, I.A. Tyapkin, N.A. Filatova, E.N. Tsyganov, M.D. Shafranov, D.I. Sherstyanov, and D. Yavorska, JINR communication 1-84, Dubna (1984). English Translation: Fermilab FN-429 (1986).

24. C.R. Sun, R.A. Carrigan, Jr., T.E. Toohig, and D. Neuffer, Proc. of the 1984 Summer Study on the Design and Utilization of the SSC, p. 483 (Snowmass - 1984).

25. A. De Rujula, S.L. Glashow, H.R. Wilson, and G. Charpak, Phys. Rep. 99, 341 (1983).

26. R.A. Carrigan, Jr., Fermilab FN-80/45 (1980); R.A. Carrigan, Jr., p. 101 in "Silicon Detectors for High Energy Physics," T. Ferber, Ed., Fermilab, Batavia (1981).

27. C.R. Sun and X. Lou, private communication.

28. L. Pondrom, Proc. of the 1982 DPF Summer Study on Elementary Particle Physics and Future Facilities, ed. by R. Donaldson, R. Gustafson, F. Paige, Snowmass, CO (1982),

p. 98.

29. I.J. Kim, Nucl. Phys. B229, 251 (1983).

FIGURE CAPTIONS

Fig. 1 Planar potential for 10 GeV protons moving in a silicon crystal for the (110) plane. The bending radius is 10 cm. The original potential W(y) is modified by the addition of a centrifugal potential. Taken from Kudo[9].

Fig. 2 Effect of skew planes on axial bending as illustrated by Bak, et al.[3] for 12 GeV/c particles. One part of the incident beam is bent 20 milliradians vertically following the (110) plane that contains the bending. Skewed (110) and (112) planes produce less net deflection as well as an x component. These data are cut on the angular region from 2.5 to 3.5 times the axial critical angle. Nearly all particles within the axial critical angle follow the (110) skew planes. The horizontal and vertical axes are in milliradians.

Fig. 3 Phase space ellipse in the NE beam at Fermilab. Half maximum curves are shown. The first panel shows the ellipse near the E711 experiment target, the second at the crystal 30m downstream. The vertical lines in the second panel show crystal angular scans. The crystal angular acceptance is shown in the second panel.

Fig. 4 Dependence of the dechanneling length ($x_{1/2}$ in millimeters) on the radius of curvature for E = 10 GeV (1) and 20 GeV (2) particles based on an averaged electron density and a (110) plane in silicon. Case (3)

shows a more realistic potential for 10 GeV. The figure is taken from Taratin, et al.[8,11] with the y axis multiplied by 6.28 to reflect only dechanneling by valence electrons as discussed in Taratin and Vorobiev[12].

Fig. 5 Dechanneling half length as a function of energy. (1) is for a straight channel, (2) for R=1m, (3) for R=0.1m. The figure is from Taratin and Vorobiev[12].

Fig. 6 Dechanneling length as a function of beam angular divergence normalized to the critical angle. From Taratin and Vorobiev[12].

Fig. 7 Behavior of the ordinary dechanneling length (1/e) with kinetic energy. (The high energy points are plotted at momentum values since they are for mixed beams. There is only a small error in doing this.) The curves are based on the Ohtsuki[13] calculation of the dechanneling length. The relativistic extrapolation is shown for both pions and protons. The dots are Campisano, et al.[14] and the crosses are Feldman, et al.[15] The CERN point is from Bak, et al.[3] and the Dubna point is based on the work of Sun[16]. The points from 40 to 200 GeV are based on an analysis of the Fermilab data by Forster[17]. With the exception of the Dubna point, all cases are Si (110). Note that the low energy points are for pencil beams while the high energy points are for a broadly illuminated channel. The dash-dot line shows the

equivalent dechanneling length for a broadly illuminated channel as estimated by Tarantin and Vorobiev[12].

Fig. 8 Number of counts as a function of crystal length after the point of maximum bend. This illustrates the approximate exponential behavior of dechanneling. From Sun et al[16].

Fig. 9 Distribution of outgoing particle directions in the Fermilab experiment[4] with small energy loss in the detector for an 8 milliradian bend in a 3-point bender. Note the peak at approximately 4 milliradians that develops as the energy is increased.

Fig. 10 Comparison of dechanneling fraction as a function of p/R, where p is the particle momentum and R the radius of curvature. The theoretical curves are taken from Ellison[9] for the (111) plane in silicon. The right curve is for the wide planes with no charge smearing while the left curve includes charge smearing and is averaged over planes. Kudo's[9] calculation for Si(110) lies more or less in between these two curves. Experimental points are based on the losses at the middle pin in the three-point bender used in the Fermilab experiment[4]. The point predicted by the Tsyganov centrifugal-force calculation for the charge-smeared case, is indicated by CF. The linear curve marked (I) is the interpolation curve used in the following figures.

Fig. 11 Phase space of the crystal acceptance (solid oval) for channeling of particles incident between two crystal planes and within the critical angle to the planar direction (dashed rectangle). Taken from Wijayawardana[4].

Fig. 12 Transmission as a function of crystal length for a sequence of momenta. The curves are for a fixed bend of 10 milliradians with a three-point bender, a 1 mm thick crystal, and an incident beam with an emittance of 0.03π cm mrad. 5 mm of the crystal is assumed to be outside of the bend.

Fig. 13 Transmission as a function of angle for a 4.5 cm long crystal. The conditions are the same as Fig. 9.

Fig. 14 Photoelastic stress pattern in a beam with a concentrated load at the upper center point. Taken from Frocht[11].

Fig. 15 Local curvature across the center of a crystal in a three-point bender (solid line). The global curvature, a constant, is also shown (dotted) as well as the total curvature (dot-dash). The y axis on the right side also shows the local efficiency (based on the total curvature) divided by the global efficiency. The curves are for a 400 GeV/c beam on a 2 mm thick silicon crystal in a three-point jig with an outer pin spacing of 5 cm.

Fig. 16 Integrated local efficiency (based on the total radius of curvature) divided by the global efficiency as a function of crystal thickness for a series of momenta. The bending conditions are the same as in Fig. 15.

Fig. 17 Bending device for the Fermilab MB crystal septum. The 0.6 mm thick crystal is visible on the left. The differential screw to adjust the bend is at the bottom. The goniometer motor (not visible) adjusts the crystal attack angle about a horizontal axis. The beam is incident from the left and is bent down. A schematic of the bending device is also shown.

Fig. 18 Crystal alignment curve at 400 GeV/c for the Fermilab M-B septum. The crystal angle is taken relative to the beam direction based on a survey. The width (100 μrad fwhm) is determined by the beam divergence.

Fig. 19 A sketch of the energy loss spectrum of the crystal detector mounted in between the two septum magnets during the crystal septum tests in the Meson Laboratory Front End Hall at Fermilab. The small hump at the center is the expected Landau peak superimposed on a large background due to the particles that are coming from other beamlines. From Wijayawardana[4].

Fig. 20 Beam optics for 200 GeV/c crystal septum operation without quadrupole magnets. Upper and lower solid lines are the paths of horizontal and vertical rays starting from the crystal with maximum angular divergence (on

momentum-off axis). The broken line is the momentum dispersion for ±5% change in momentum (off momentum-on axis). From Wijayawardana[6]. (Note that the scale is distorted.)

Fig. 21 Beam optics for 400 GeV/c crystal septum operation with horizontal point-to-point focusing and momentum recombination. Upper and lower solid lines are the paths of the horizontal and vertical rays starting from the crystal with maximum angular divergence (on momentum-off axis). The broken line is the momentum dispersion for a ±5% change in momentum (off momentum-on axis). From Wijayawardana[6]. (Note that the scale is distorted.)

Fig. 22 Plan view of the NE beam at Fermilab. E711, the high intensity experiment is upstream of the crystal; E653, the low intensity experiment, is downstream. The crystal 30m downstream of the E711 target replaced forty feet of bending magnet. Note the beam dump 20m downstream of the crystal. (Note that the scale is distorted.)

Fig. 23 Goniometer scan over the plane in the NE beam at Fermilab. One goniometer step is 5 microradians. The width is 46 microradians FWHM.

Fig. 24 Beam profile downstream of the NE septum at Fermilab. The upper part is the vertical profile, the lower part is the horizontal. Each bar is 1 mm wide. Note that

the beam is less than 2mm wide horizontally.

Fig. 25 Schematic layout for crystal extraction from the Dubna synchrophasotron. The crystal (2) is located in the first straight section (1). There is a target at 3. The first quadrant of the accelerator is 4. The experimental hall is at 5[23].

Fig. 26 Dependence of the extracted beam intensity on crystal orientation for the Dubna crystal extraction septum[23]. The ordinate is the S_2 counter singles rate per spill in units of 10^5. The horizontal axis is the angle between the crystal and the accelerator beam and ranges from -3 to +3 milliradians. The background is due to secondary radiation. The upper panel is at 4.2 GeV, the middle at 6.0 GeV and the bottom at 7.5 GeV.

Fig. 27 Seagoing 2 TeV accelerator proposed by De Rujula, et al.[25] for neutrino exploration of the center of the earth. The diameter of the ring might be 2-4 Km. A tungsten crystal might be able to replace both the extraction and bending portion of the device.

Fig. 28 Schematic illustration of a possible focusing element using bent crystals. A parallel beam with angular dispersion less than the critical angle could be focused almost to a line in one direction. A second element in the other direction could focus to a point.

Fig. 29 Test jig for crystal compression studies for a possible quadrupole crystal element. The jig was constructed and operated by Sun and Lou[19]. The wedge at the top is used to achieve small vertical compressions on the crystal near the bottom in the sandwich.

Fig. 30 A possible "separated" charm-particle beam. All the particles within the critical angle are bent. Most of the charm particles decay in the straight section. Long-lived particles continue around the bend.

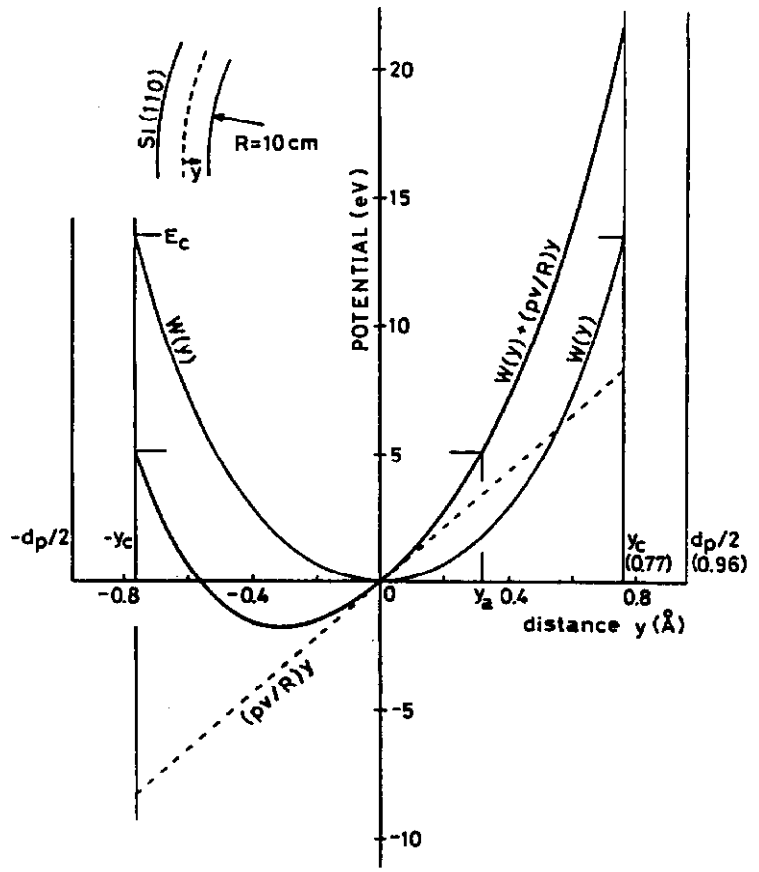

Figure 1

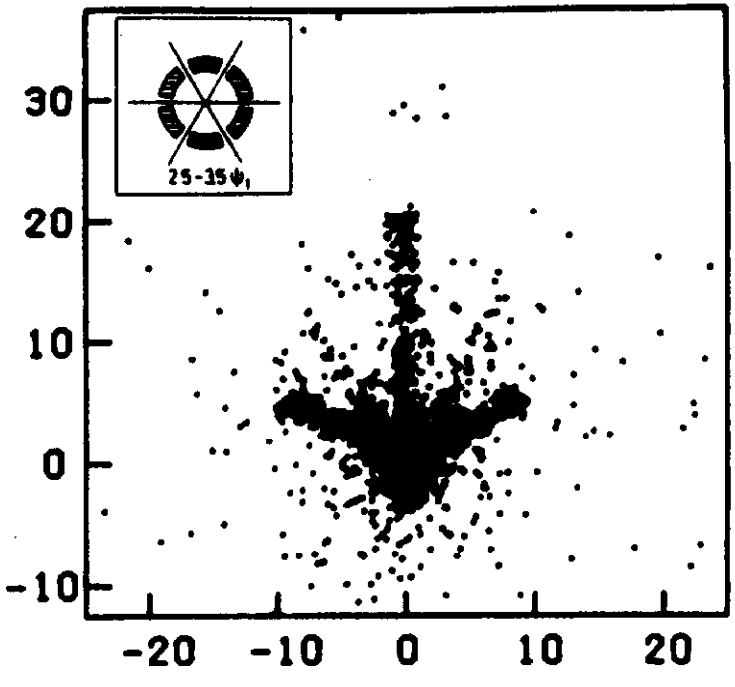

Figure 2

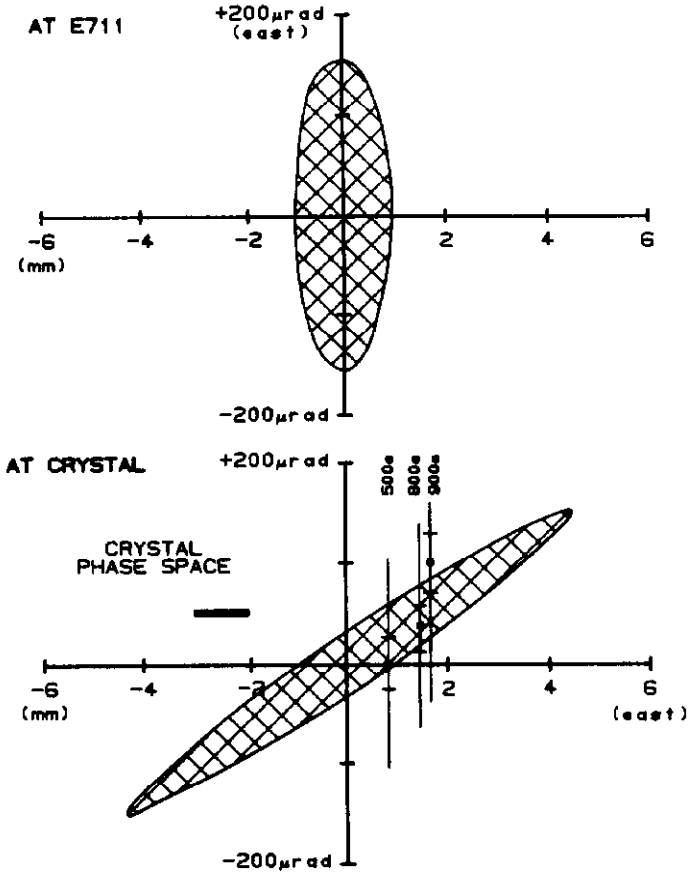

Figure 3

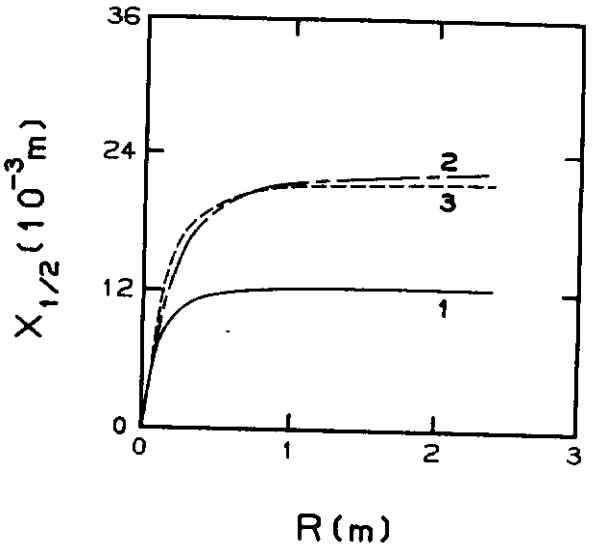

Figure 4

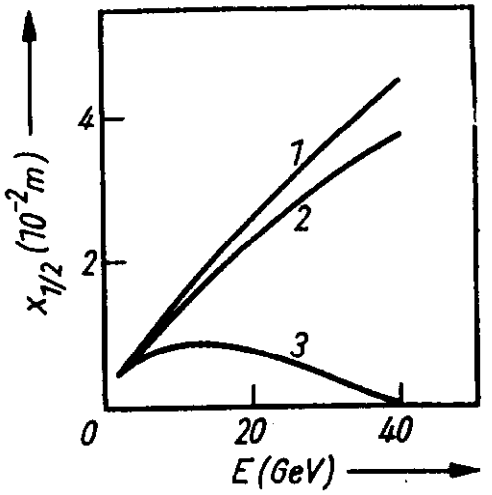

Figure 5

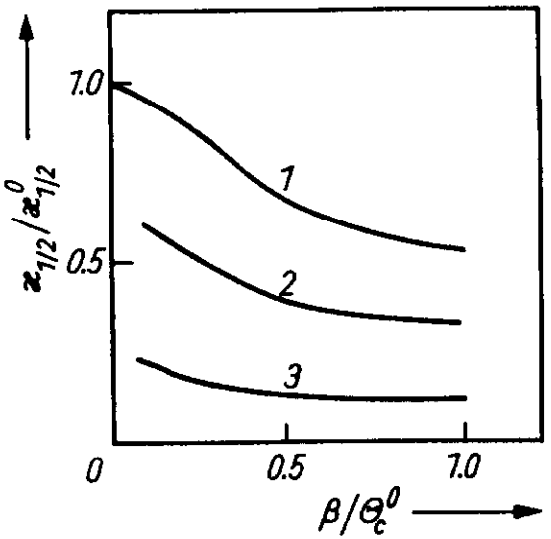

Figure 6

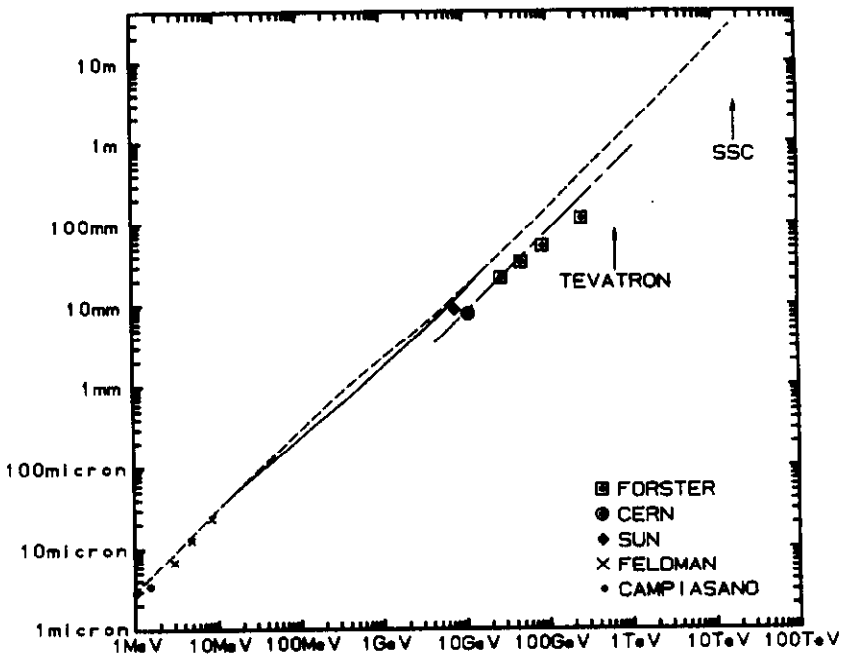

Figure 7

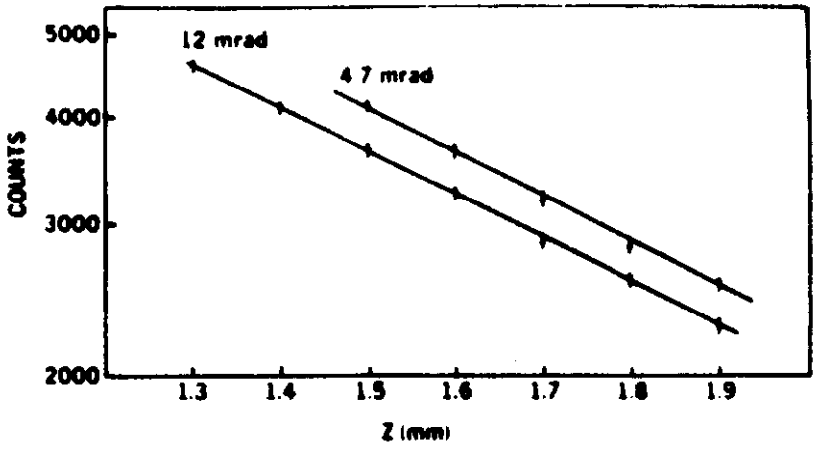

Figure 8

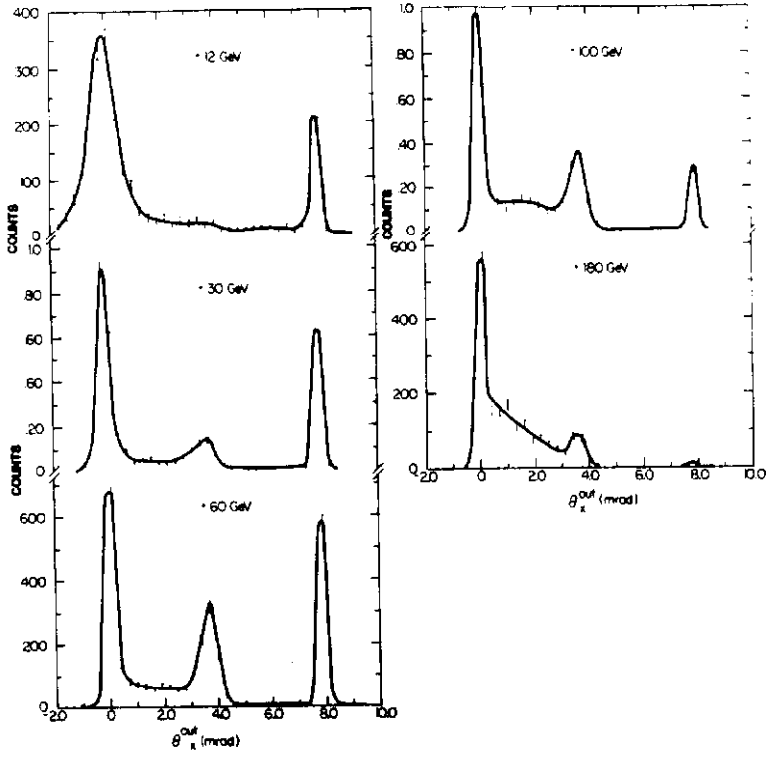

Figure 9

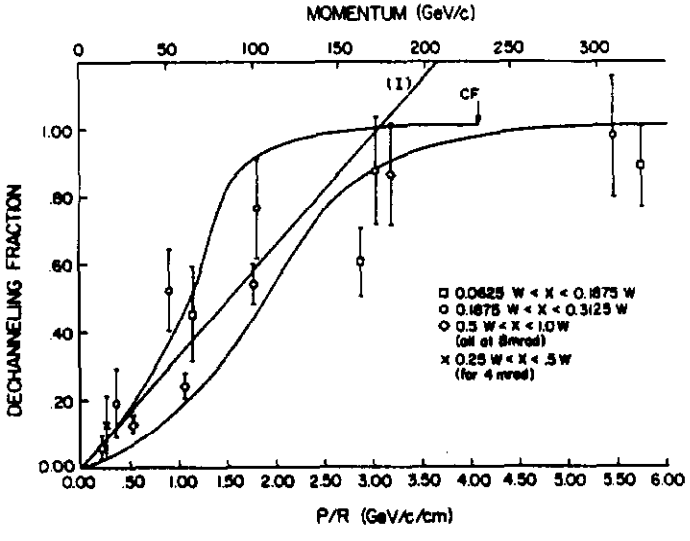

Figure 10

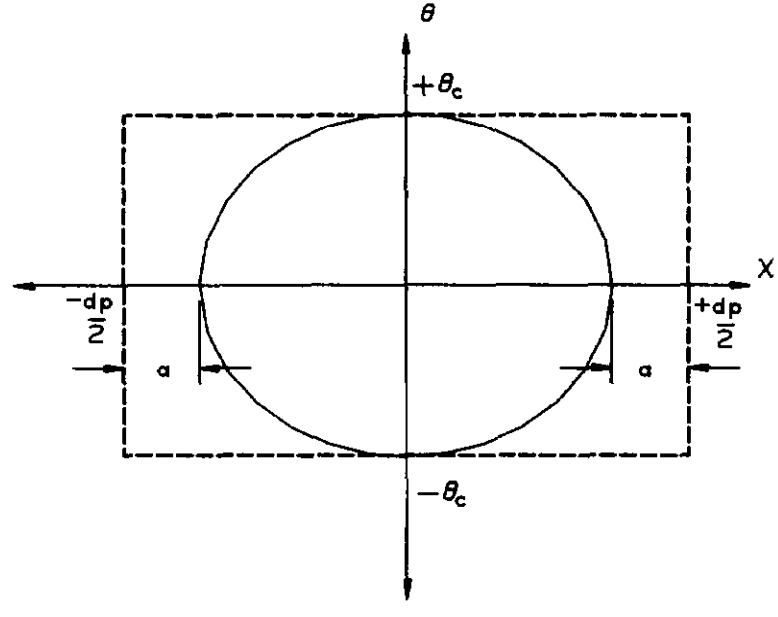

Figure 11

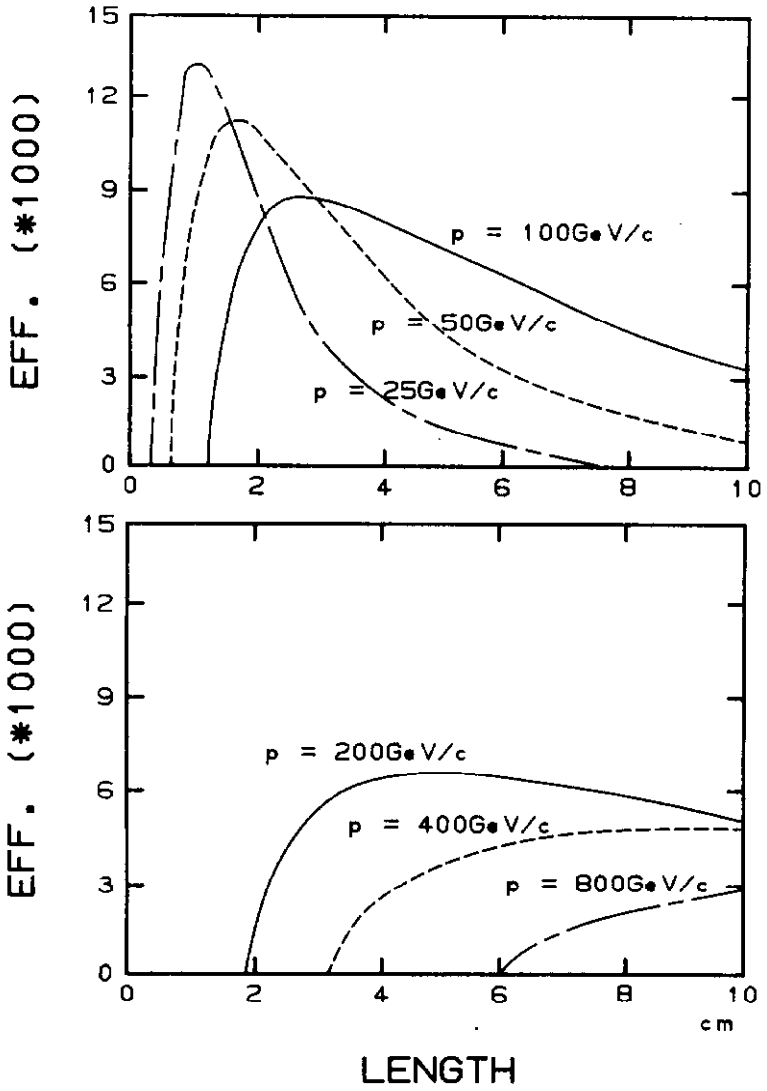

Figure 12

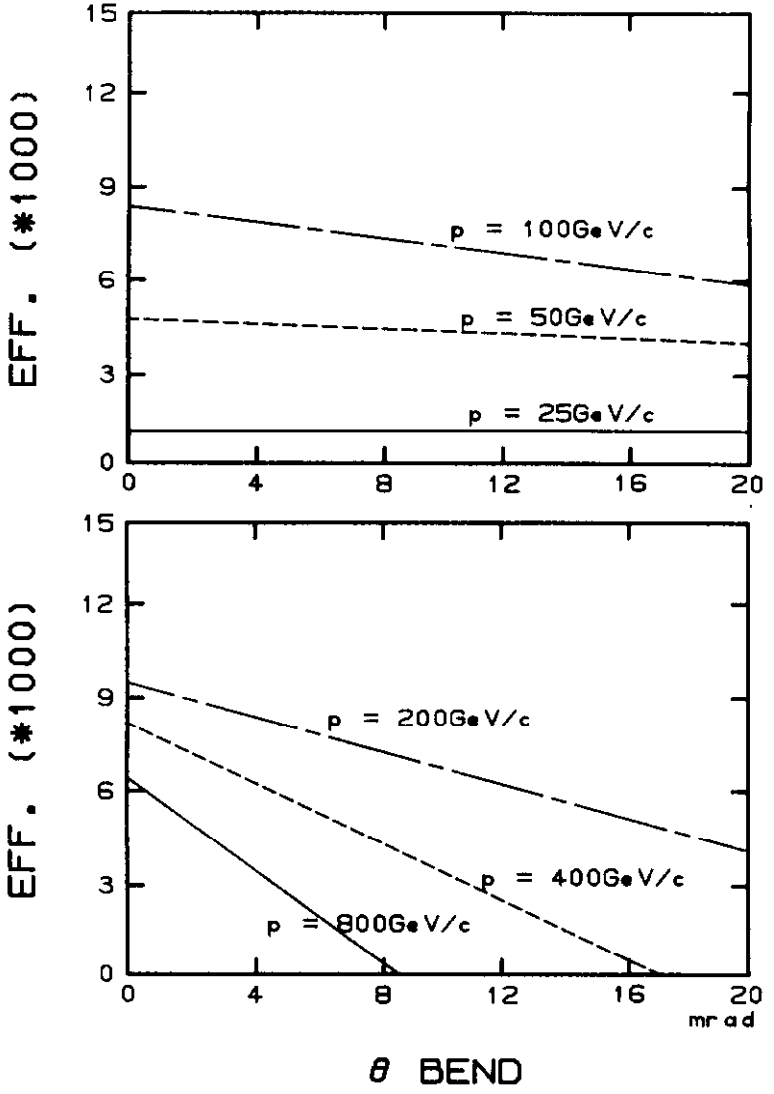

Figure 13

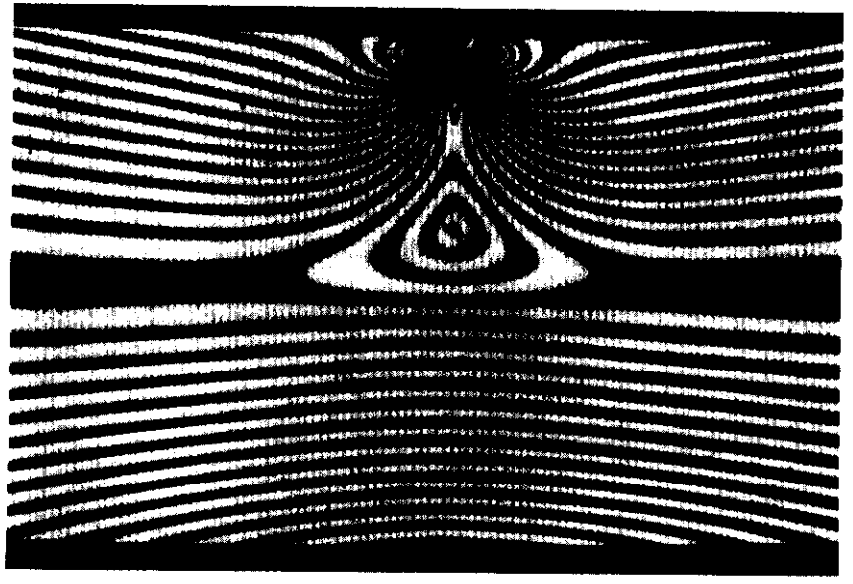

Figure 14

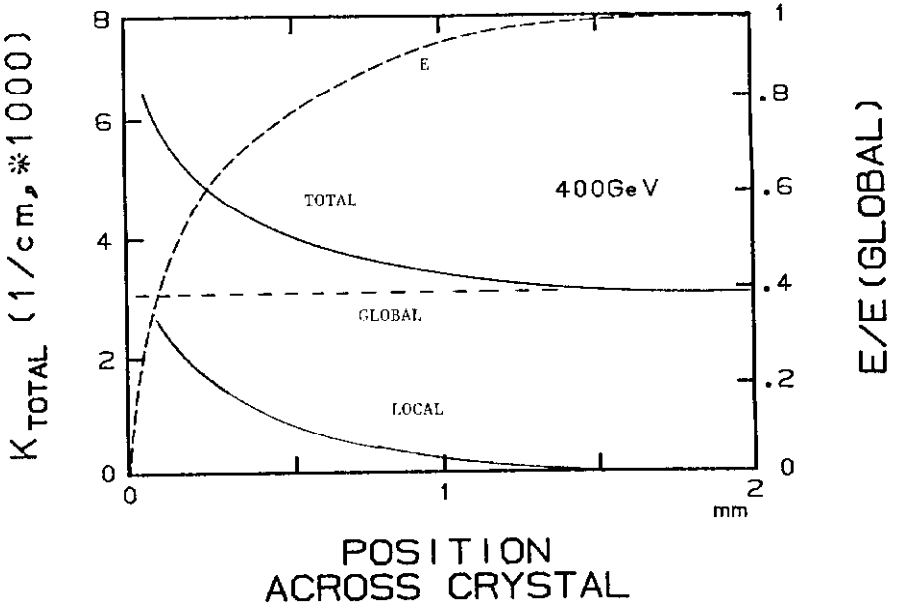

Figure 15

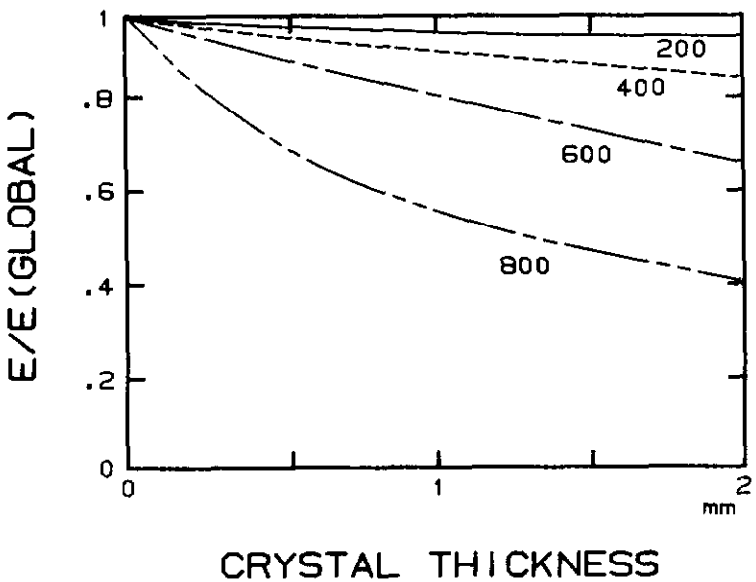

Figure 16

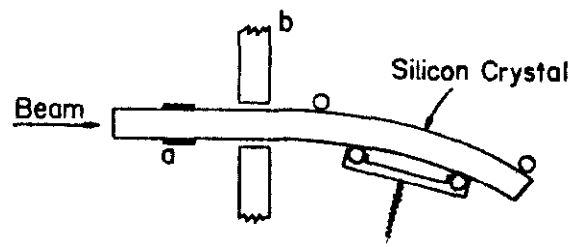

Figure 17

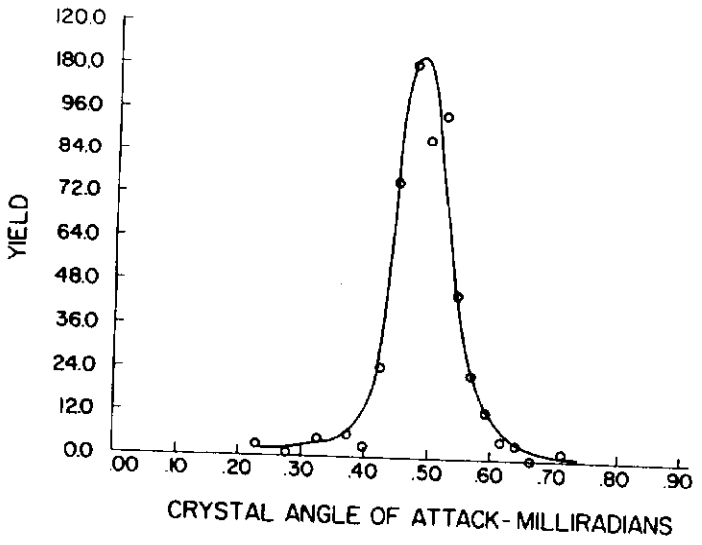

Figure 18

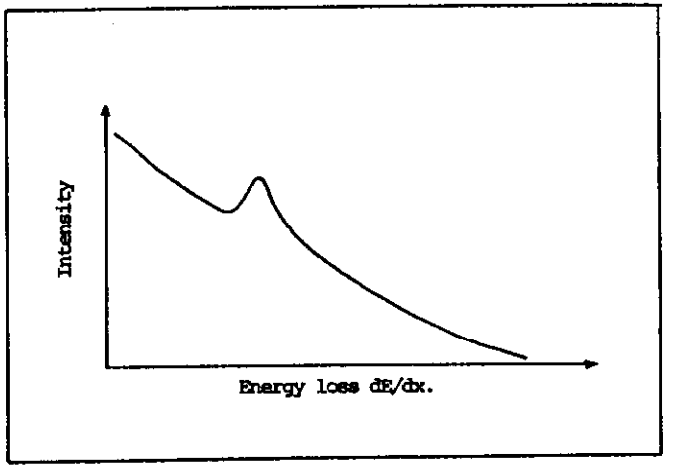

Figure 19

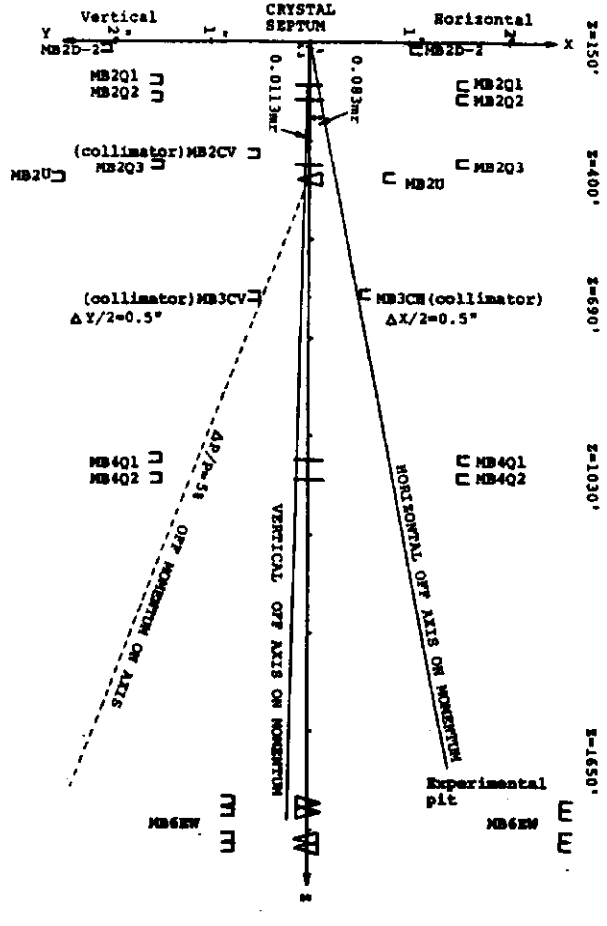

Figure 20

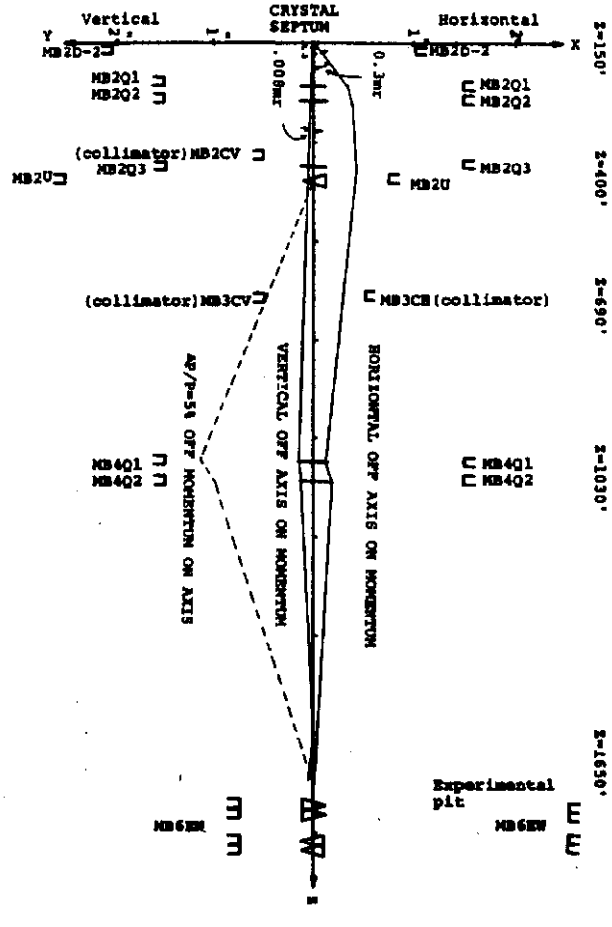

Figure 21

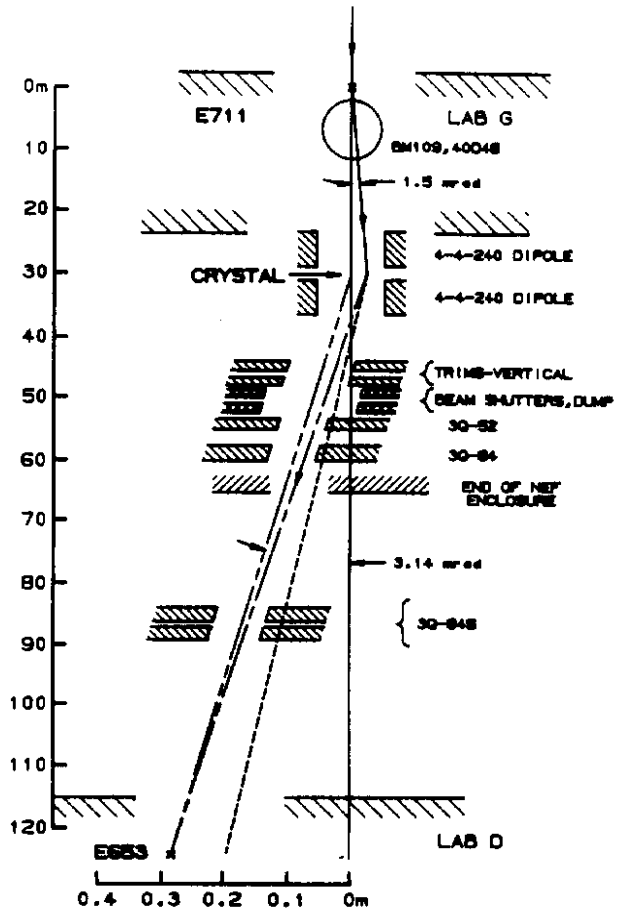

Figure 22

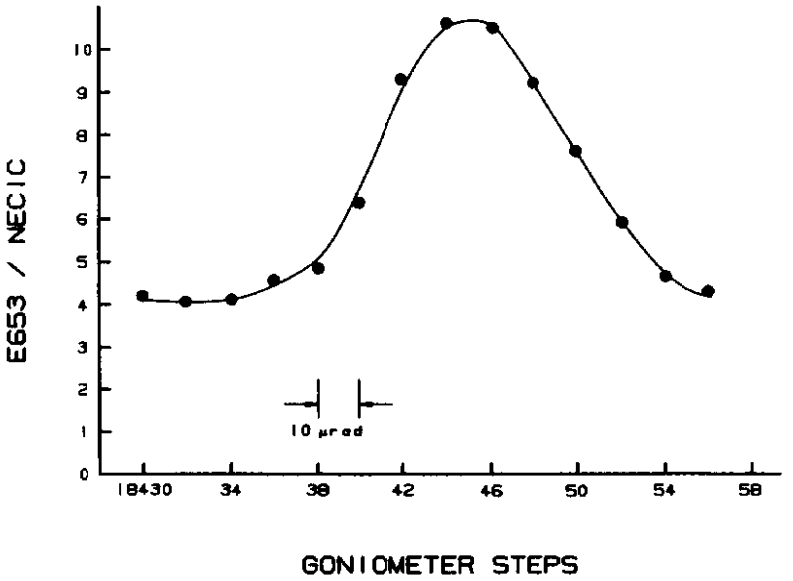

Figure 23

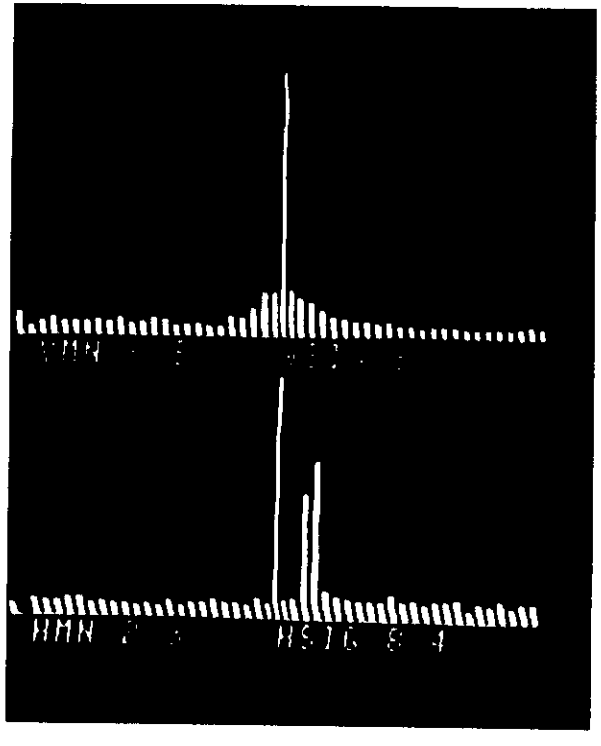

Figure 24

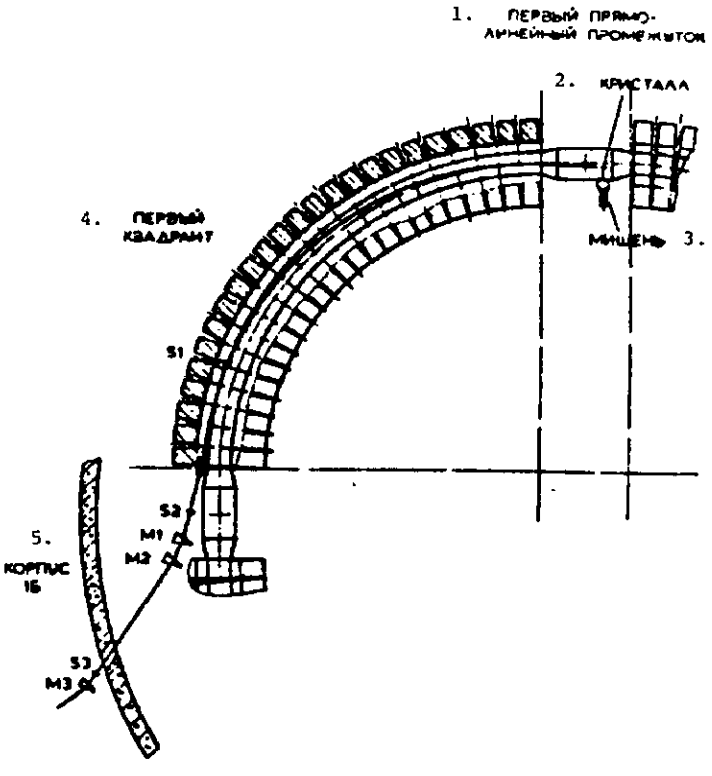

Figure 25

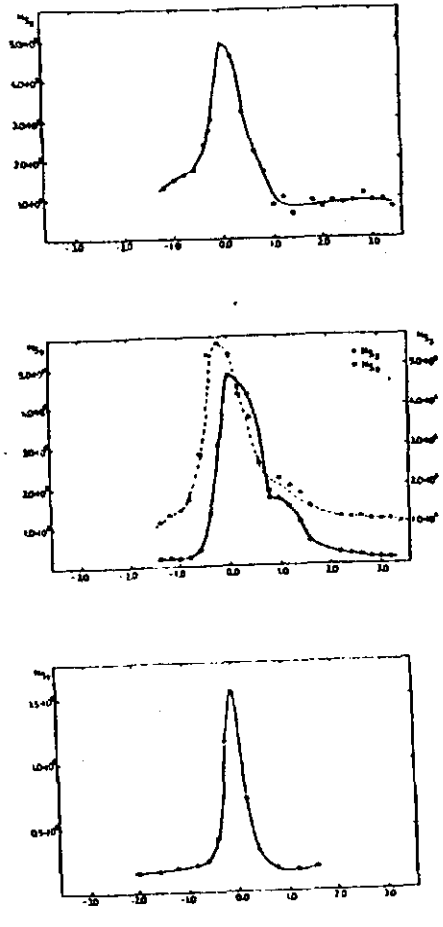

Figure 26

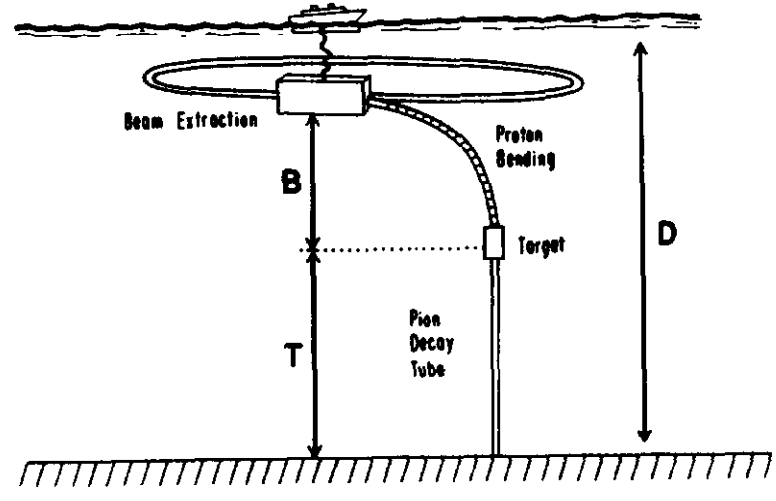

Figure 27

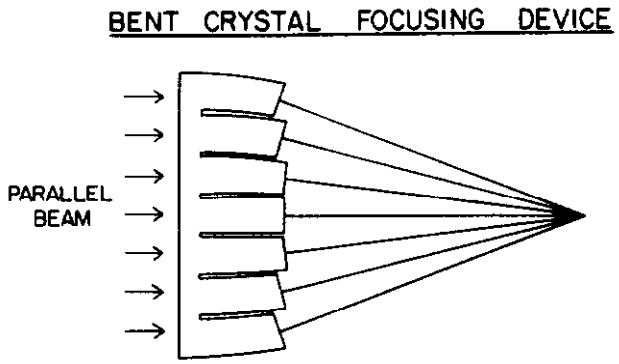

Figure 28

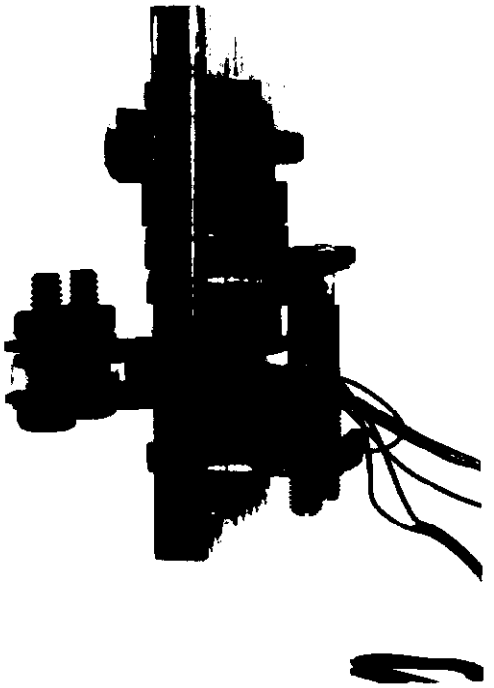

Figure 29

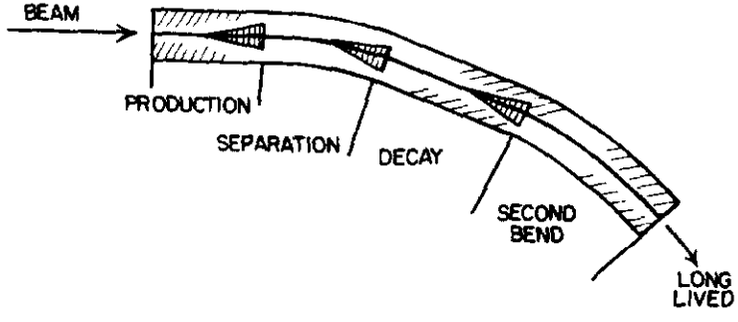

Figure 30